Orbital Angular Momentum Reversal and Asymmetry in Acoustic Vortex Beam Reflection

Zheguang Zou⬤, Robert Lirette⬤, and Likun Zhang⬤*

National Center for Physical Acoustics and Department of Physics and Astronomy, University of Mississippi,
University, Mississippi 38677, USA

We present acoustic modeling, measurements, and interpretation of the angular momentum carried in an ultrasonic vortex beam that is obliquely reflected off a flat water-air interface. The experimental measurements observe the theoretically predicted reversals of phase rotation, topological charge, and orbital angular momentum in a reflected vortex beam in direct analogy to optical phenomena. The spatial and temporal evolution of the linear and angular momentum during the reflection are determined by calculating the velocity field from two-dimensional scanned pressure fields. A conversion of the angular momentum indicates a radiation torque along the oblique reflecting surface. We understand this radiation torque originates from the break of rotational symmetry with respect to the incident plane for normal components of the energy flux and linear momentum density at the reflecting surface. Our study provides mechanical evidence on the effect of a flat surface on the reflection of vortex beams and gains insight into the underlying physics, impacting non-contact manipulation of objects and communication.

The law of reflection states that the direction of reflected light is in the plane of incidence, and the angle of reflection equals the angle of incidence. Nevertheless, the law of reflection is not enough to describe angular momentum carried by reflected vortex beams. Vortex beams with a twisted wave front, stemming from an azimuthal dependency $\exp(il\phi)$ (ϕ the azimuthal angle), carry orbital angular momentum (OAM) that is quantified by the topological charge l (integer) for any type of waves (including acoustic [1,2], optical [3], and electron [4]). In the fundamental problem of optical vortex beam reflection from a flat surface [5–8], the vortex phase rotation and OAM carried by the reflected beam reverse their direction in reference to the propagating direction resulting in an opposite topological charge $-l$. This phenomenon of topological charge and OAM reversals implies a nondissipative radiation torque on the reflecting surface upon the reflection of an obliquely incident vortex beam (Fig. 1). The reflected beam can be deflected out of the plane of incidence when using an intense laser beam, deviating the optical reflection law, as modeled in [6] or in [9] for circularly polarized laser beams carrying spin angular momentum. In this Letter, we report our experimental measurements on phase rotation and OAM in oblique reflection of acoustic vortex beams from a flat interface and explore the underlying physics. Our experimental measurements, theoretical model, and interpretation provide mechanical evidence of the opposite phase rotation and OAM reversal in reflected vortex beams and gain insight into the resultant radiation torque on the oblique reflecting surface.

Here there is no energy absorption associated with the conversion of angular momentum, differing from the
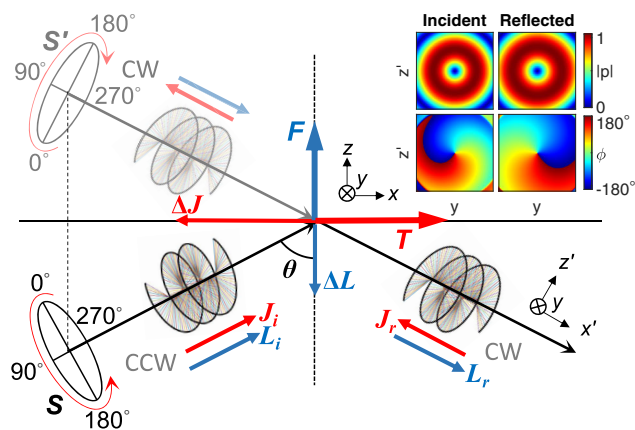

FIG. 1. Schematic illustration of the total reflection of an acoustic vortex beam. A counterclockwise (CCW) vortex beam (with linear momentum L_i and angular momentum J_i) generated by a source array S (consisting of a circle of N point sources, each with $2\pi/N$ vortex phase increment defined in our code), is obliquely incident to the interface at an angle θ. Following from the method of images, the reflected beam (with L_r and J_r) extended from the virtual source S' rotates clockwise (CW). During the reflection, change of linear momentum $\Delta L = L_r - L_i$ yields an acoustic radiation force F, and change of angular momentum $\Delta J = J_r - J_i$ exerts a torque T at the interface. The inset shows numerically modeled acoustic pressure amplitude (normalized) and wave phase at planes normal to the propagating direction for incident and reflected vortex beams (the source number is $N = 16$).

radiation torque spinning an axisymmetric object by vortex beams where the transfer of angular momentum is accompanied by energy absorption [2,10–12] (see experiments in [13–25]). Furthermore, the radiation torque of concern here is not along the beam direction and disappears in the normal incidence. This differs from another category of nondissipative OAM conversion that occurred when using a spiral phase plate to convert an ordinary wave into a vortex beam, where the OAM conversion and resulting radiation torque on the structure should be along the beam direction and normal to the plate (via either reflection [26] or transmission [27] or diffraction [28–30]). Lastly, the torque concerned here also differs from the average torque on a Rayleigh disk exerted by an ordinary wave carrying no OAM [31,32]. The analogy between optical waves and acoustic waves has been well emphasized in their carried linear and angular momentum and interactions with matter [2,15,33,34]. The radiation torque on obliquely reflecting interface explored herein due to asymmetry of acoustic radiation pressure of obliquely incident vortex beams is also analogous to optical phenomena [6,9].

Mechanism and modeling.—In general, wave reflection follows Huygens principle—the wave front of reflected waves is a sum of all waves advancing from new sources at each reflecting point. When considering reflection of a point source from a flat surface, this process is simplified to specular reflection. The reflected path extends from an imaginary source located on the other side of the interface. The method of images provides a quick approach to examine the reflection of vortices using point sources (Fig. 1). Consider a source array S consisting of a circle of N identical point sources, each with a $2\pi/N$ initial phase increment forming a counterclockwise vortex beam with a topological charge of $+1$. Using the method of images, the imaginary source array S' forms a reversed phase pattern and a clockwise rotation. The reflected beam, extending from S', has a clockwise phase rotation opposite to the original vortex beam. Thus, the phase pattern, rotation direction, and topological charge are all reversed from the incident to reflected vortex beams in reference to propagating direction. Whereas the illustration in Fig. 1 is for a hard boundary, this phase reversal remains after accounting for an additional 180° phase shift if reflecting from a soft boundary.

Following wave propagation and phase rotation, the linear and angular momentum can be obtained (Fig. 1). While a reversed vertical wave propagation direction suggests a reversal of linear momentum normal to the reflecting surface, a reversed phase rotation direction suggests a reversal of angular momentum parallel to the reflecting surface. Angular momentum is linked with phase rotation such that the direction of angular momentum is along the wave propagation direction before reflection but against the wave propagation direction afterward. For a total reflection with an incident angle θ, the change in linear momentum is $\Delta L = L_r - L_i = 2L_i \cos\theta$ and normal to the surface, while the change in angular momentum is $\Delta J = J_r - J_i = 2J_i \sin\theta$ along the surface, where the subscripts i and r denote the incident and reflected waves, respectively. The change of angular momentum reduces to zero in normal incidence.

We simulated the obliquely incident and reflected acoustic vortex fields using the above N point source model. We used $N = 16$ for modeling to qualitatively mimic the vortex feature of our 16 segment vortex lens in experimental measurements. To be comparable with our transducer, the frequency is set to 0.9 MHz, and the sources are located in a circle of a radius 15 mm. The acoustic pressure field emitted by the nth point source takes the form of spherical waves: $p_n(\vec{r}) = p_0 \exp[i\vec{k}(\vec{r} - \vec{r}_n) + il\phi_n]/|\vec{r} - \vec{r}_n|$, where the time dependency $\exp(-i\omega t)$ (where ω is the angular frequency, and t is the time) is omitted, p_0 is the pressure amplitude, $\vec{k}$ is the wave number, $\vec{r} = \vec{r}(x, y, z)$ is the field location, and $\vec{r}_n$ and ϕ_n are the source location and initial phase, respectively. Applying the method of images, the reflected beam is modeled with imaginary source located at $\vec{r'}_n(x, y, -z)$. The total acoustic field is a sum of fields from all point sources $p = \sum p_n$. The numerical model consisted of superimposed spherical waves calculated within MATLAB using a fine spatial resolution of 0.01 mm (about 1/166 acoustic wavelength). Our modeling results (inset of Fig. 1) show that in the planes normal to the wave propagation direction, the phase pattern, topological charge, and angular momentum density are all reversed after reflection, confirming the theoretical prediction.

Experimental observations and modeling comparison.— The experiment was conducted underwater to observe the incident and reflected fields of vortex beams reflecting off a flat water-air boundary. The boundary exhibits total reflection by a mismatch of the acoustic impedance on the order of 10^3. The setup of our experiment is in Fig. 2(a). The incident and reflected acoustic fields from a vortex beam generating transducer were mapped using a machine controlled hydrophone scan tank. The dimensions of the experimental tank are $65 \times 65 \times 32$ cm^3 (L × W × H), and it was filled with distilled water up to a height of 25 cm. The source transducer was an Olympus V302 spherically focused acoustic transducer with a measured center frequency of 0.9 MHz and a 50.8 mm focal length. The source was positioned at a depth of 30 mm below the water surface, oriented upward toward the water-air boundary at $\theta = 45°$. A Precision Acoustics 0.5 mm diameter needle hydrophone was initially positioned 40 mm from the transducer along the axis and at a depth of 10 mm below the surface.

The acoustic vortex was generated using an 3D printed phase-plate lens with 16 phase step increments [Fig. 2(b)]. This lens allows the generation of vortex beams with a topological charge of -1. The precise location of the hydrophone was controlled via code written in MATLAB.
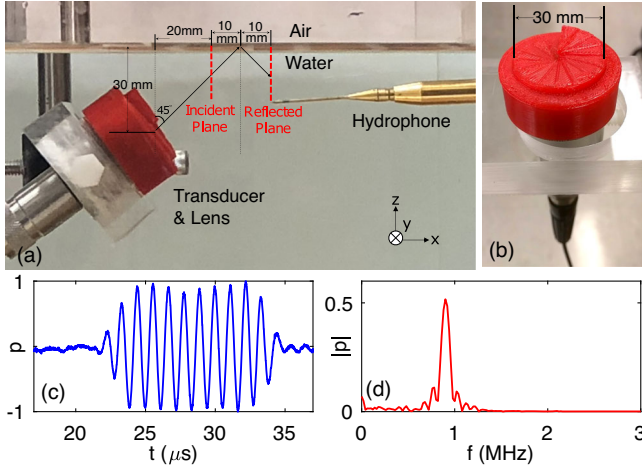
FIG. 2. Experimental setup. (a) Photo of the experimental setup. The scan areas for the incident and reflected are both 20 mm × 20 mm center at the depth of 10 mm. (b) Acoustic transducer with the 16 segment vortex lens. (c) Example of a received acoustic signal, where the time is relative to the source. (d) Frequency spectrum of the signal in (c), indicating a central frequency of 0.9 MHz.
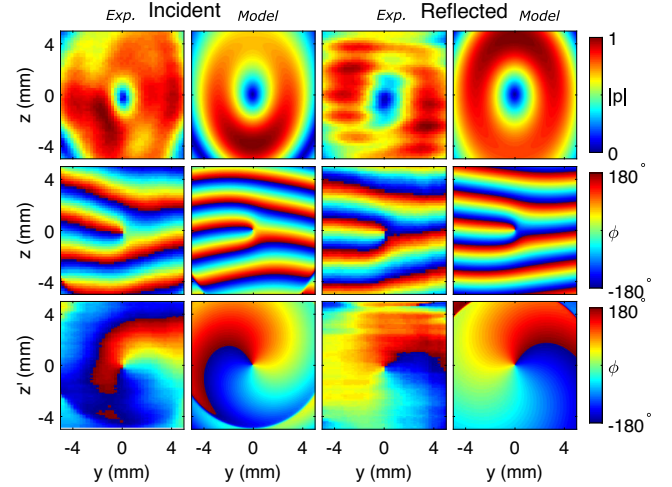

FIG. 3. Comparison of experimental measurement (denoted by *Exp.*) with numerical model for the normalized acoustic pressure amplitude (top panels) and phase (center panels) at the scanning planes for both the incident and reflected beams. Bottom panels: projection to planes normal to propagation direction (see text).

Our interest was to measure reversals of the vertical component of linear momentum (normal to the reflecting surface) and the horizontal component of angular momentum (parallel to the reflecting surface), both of which can be resolved from vertical 2D planes (y-z plane). The vertical planes are relatively easy to align in comparison with tilted planes normal to propagating directions. We scanned two vertical planes, 20 mm axially away from the transducer for incident and 40 mm away for reflection. At each axial location scans were taken over a vertical 20 × 20 mm plane. The vertical and horizontal scan resolutions are 0.25 mm each. The transducer was driven by a burst of 10 cycles of a 0.9 MHz sinusoid, which was repeated every 5 ms. A burst source was used to minimize standing waves in the tank and overlap of the desired data from secondary reflections. The resulting data was averaged over 16 wave forms. An example of the received acoustic signal is shown in Fig. 2(c), whose spectrum is further shown in Fig. 2(d).

We output the complex pressure fields at the central frequency from the 0.9 MHz spectral component of the fast Fourier transform of the measured signals. As shown in Fig. 3, the amplitude fields are in toroidal shapes, slightly elongated due to an oblique projection. The amplitude minimum at the center indicates the singularity of the vortex beam. The phase patterns are in stripes because our scanning planes are not normal to the wave propagation direction. Using a hologram algorithm, it is possible to move this oblique projection to the one normal to the propagation direction. A projection following from propagation in the paraxial approximation is shown in Fig. 3. The rotation direction of the vortex beam is determined from the wave phase reduction near the singularity. From our

experimental results, we observed that the incident and reflected phase patterns are reversed, as theoretically predicted. The incident beam rotates clockwise and the reflected one rotates counterclockwise, confirming the reversals of phase pattern and rotation direction upon reflection.

The results following from our numerical model, which uses 16 point sources (like inset of Fig. 1 but now for a source with a topological charge of −1), are also shown in Fig. 3 for qualitative comparison. Our modeling results show close agreement with measurements, including stretched toroidal shapes, striped phase patterns, and correct rotation directions of vortex beams before and after the reflection. The interference pattern seen in the experimental results after the reflection stems from the superposition of the incident and reflected waves but is not seen in the modeling, which does not include the superposition.

Angular momentum reversal and asymmetry.—We determined the linear momentum and angular momentum from experimentally scanned acoustic pressure fields. The angular momentum density follows from the linear momentum density with $\vec{J} = \vec{r'} \times \vec{L}$, where $\vec{r'}$ is the location relative to the center of the vortex beam found via searching the minimum of pressure amplitude near the vortex center. The linear momentum density for acoustic waves is given by $\vec{L} = p\vec{u}/c_0^2$ (where c_0 is the sound speed), requiring calculation of the velocity field $\vec{u}$ from the pressure p.

We calculated the ith component of $\vec{u}(t)$ via a spatial gradient and then the time integral of the scanned pressure $p(t)$ as follows:

$$u_i(t) = -\frac{1}{\rho_0} \int_0^t \frac{\partial p(t)}{\partial x_i} dt, \tag{1}$$
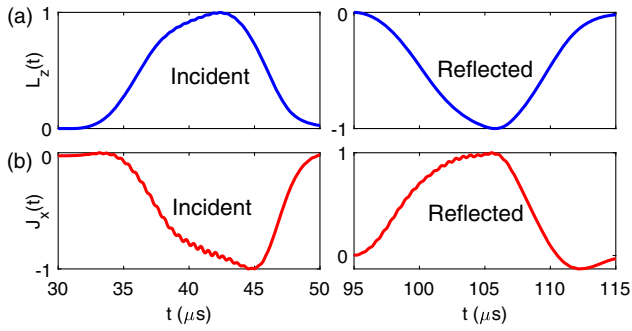
FIG. 4. Experimental results of the temporal evolution of (a) vertical linear momentum L_z and (b) horizontal angular momentum J_x contained in the scanned planes, exhibiting reversals from the incident (left) to reflected (right) field. The values have been normalized to their own maximum.

which follows from the equation of motion $\rho_0 \partial \vec{u}/\partial t = -\vec{\nabla} p$, where ρ_0 is the medium density and u_i is the velocity component in the x_i axis. The spatial gradient is satisfied by our fine spatial resolution of 0.25 mm in the scan, which is about 1/7 of the wavelength (1.67 mm). The time integral in Eq. (1) was started with an initial pressure field before the arrival of vortex beams at the interface. The horizontal angular momentum normal to the vertical scanning plane follows from the components of linear momentum density in the scanning plane. The linear and angular momentum densities were averaged over a period corresponding to the central frequency. The total linear and angular momentum follows from the sum of the linear and angular momentum density over the entire measured plane.

Figure 4 shows our results for the time evolution of total vertical linear momentum L_z and total horizontal angular momentum J_x contained in the scanned planes. The results show that the vortex beam arrives at the incident plane at around 35 μs, and then the vertical linear momentum and horizontal angular momentum (the minus sign denotes a negative direction) both gradually increase. The angular

momentum reaches the maximum at around 45 μs. It then decreases back to zero at around 50 μs when the sound leaves the interface. Our results confirm the reversals of linear momentum along the vertical direction and, importantly, the reversal of the angular momentum along the horizontal direction. In addition, this result demonstrates the time-varying process of these reversals for acoustic vortex signals emitted from our source.

The reversal of angular momentum implies a net radiation torque at the interface due to the change in angular momentum. To interpret this torque, we examine the momentum density and radiation pressure at the reflecting interface. Consider our modeling vortex beam where the acoustic pressure amplitude p [Fig. 5(a)] and the linear momentum density L [Fig. 5(b)] at the interface are simply symmetrical with respect to the incident plane ($y = 0$). In contrast, the normal component of the momentum density L_z is *asymmetric* with respect to the incident plane [Fig. 5(c)]. This asymmetry of L_z then creates an uneven radiation pressure on the interface $P(x, y)\hat{z}$ with respect to the incident plane, leading to a net radiation torque [which is the integral of $\vec{r'} \times P(x, y)\hat{z}$ over the surface] along the $\hat{x}$ direction in the reflecting surface.

The asymmetry of the normal component of momentum density results from the corresponding asymmetry of normal projection [see the projection angle $\beta = \arccos(L_z/L)$ in Fig. 5(d)]. We understand this projection asymmetry by illustrating the twisted energy flux (and correspondingly twisted linear momentum) of the vortex beam crossing to the oblique reflecting surface [Fig. 5(e)]. The illustration displays that the twisted flux has a rotational symmetry but ends up having an asymmetric projection to the reflecting surface normal with respect to the incident plane $y = 0$ due to the tilted angle in oblique incidence. Our experimental measurements of OAM change validate this asymmetry and resultant torque in oblique reflection of vortex beams.

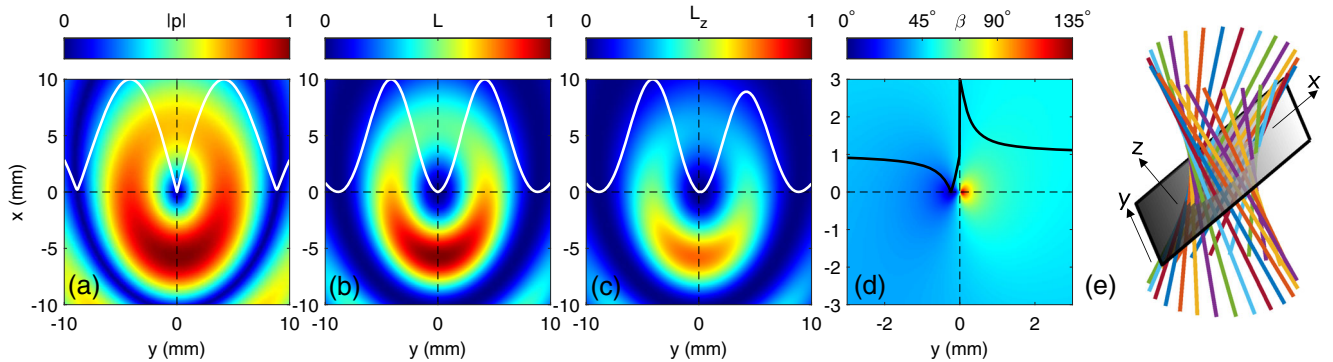*Summary and outlook.*—To summarize, we have explored the reflection of acoustic vortex beams with

FIG. 5. Symmetry and asymmetry features of a vortex beam at the obliquely reflecting interface: (a) pressure amplitude $|p|$, (b) total linear momentum density L, (c) vertical component of linear momentum density L_z, (d) projection angle $\beta = \arccos(L_z/L)$. The solid lines in each plot depict associated values along y axis ($x = 0$ mm) to highlight the symmetry in (a),(b) and asymmetry in (c),(d). The incident angle is 45°. (e) Illustration of the asymmetry feature of a symmetric vortex vector field due to an oblique projection.

model and experiment. Our experimental measurements confirmed the existence of reversal features as predicted by theory and model. Our results further imply an acoustic radiation torque at the interface, which we explain by the asymmetry of vortex features at the interface resulting from the asymmetry of the normal momentum density or radiation pressure at the reflection interface with respect to the incident plane in the case of oblique incidence. No absorption is needed for the torque to occur. Our modeling using the method of images and interpretation by vortex projection asymmetry is complementary to the studies in optics.

In communication [35–38], the topological charge is used as a new degree of freedom for multiplexing. When sending vortex beams in confined space (for example, the existence of two natural boundaries—sea surface and sea floor—for underwater communication), the sign of the topological charge will be reversed each time it interacts with the boundary. This effect together with the refraction [37] should be taken into account to resolve the correct topological charge for information demodulation. Another example is for object rotation in acoustic tweezer applications [13–25]. When manipulating a particle near a surface, we anticipate that a reversed rotation should be observed, i.e., the reversed torque after oblique reflection leads to a reversed rotation of a particle or a disk along the beam axis.

The asymmetry of radiation pressure (or resulting radiation torque) can cause a deflection of reflected vortex beam out of incident plane. A deflection in optics was recently simulated by using an obliquely incident high-intensity laser beam [6]. Due to the low acoustic power level used in our experimental setup, we were unable to directly observe the deflection of the beam or the deformation of the water-air interface. Future research will explore measurements of radiation torques with high-intensity ultrasonic vortex beams. We anticipate a sufficient radiation torque would rotate a light disk about the x axis (see Fig. 1) if the disk is placed to obliquely reflect the beam (similar to the configuration in [16,19,20]). The torque depends on the incident angle and the specific type of vortex beams. Also to be explored is the field distribution in the reflected beam [39,40].

---

*Corresponding author.
 zhang@olemiss.edu

[1] B. T. Hefner and P. L. Marston, An acoustical helicoidal wave transducer with applications for the alignment of ultrasonic and underwater systems, J. Acoust. Soc. Am. **106**, 3313 (1999).

[2] L. K. Zhang and P. L. Marston, Angular momentum flux of nonparaxial acoustic vortex beams and torques on axisymmetric objects, Phys. Rev. E **84**, 065601(R) (2011).

[3] L. Allen, M. W. Beijersbergen, R. J. C. Spreeuw, and J. P. Woerdman, Orbital angular momentum of light and the transformation of Laguerre-Gaussian laser modes, Phys. Rev. A **45**, 8185 (1992).

[4] M. Uchida and A. Tonomura, Generation of electron beams carrying orbital angular momentum, Nature (London) **464**, 737 (2010).

[5] M. Merano, N. Hermosa, J. P. Woerdman, and A. Aiello, How orbital angular momentum affects beam shifts in optical reflection, Phys. Rev. A **82**, 023817 (2010).

[6] L. Zhang, B. Shen, X. Zhang, S. Huang, Y. Shi, C. Liu, W. Wang, J. Xu, Z. Pei, and Z. Xu, Deflection of a Reflected Intense Vortex Laser Beam, Phys. Rev. Lett. **117**, 1 (2016).

[7] H. Li, F. Honary, Z. Wu, and L. Bai, Reflection and transmission of Laguerre-Gaussian beams in a dielectric slab, J. Quant. Spectrosc. Radiat. Transfer **195**, 35 (2017).

[8] Y. Yao, X. Liang, M. Zhu, W. Zhu, J. Geng, and R. Jin, Analysis and experiments on reflection and refraction of orbital angular momentum waves, IEEE Trans. Antennas Propag. **67**, 2085 (2019).

[9] Y. H. Tang, Z. Gong, J. Q. Yu, Y. R. Shou, and X. Q. Yan, Deflection of a reflected intense circularly polarized light beam induced by asymmetric radiation pressure, Phys. Rev. E **100**, 063203 (2019).

[10] L. K. Zhang and P. L. Marston, Acoustic radiation torque on small objects in viscous fluids and connection with viscous dissipation, J. Acoust. Soc. Am. **136**, 2917 (2014).

[11] L. Zhang, Reversals of orbital angular momentum transfer and radiation torque, Phys. Rev. Appl. **10**, 1 (2018).

[12] I. D. Toftul, K. Y. Bliokh, M. I. Petrov, and F. Nori, Acoustic Radiation Force and Torque on Small Particles as Measures of the Canonical Momentum and Spin Densities, Phys. Rev. Lett. **123**, 183901 (2019).

[13] K. Volke-Sepúlveda, A. O. Santillán, and R. R. Boullosa, Transfer of Angular Momentum to Matter from Acoustical Vortices in Free Space, Phys. Rev. Lett. **100**, 024302 (2008).

[14] K. D. Skeldon, C. Wilson, M. Edgar, and M. J. Padgett, An acoustic spanner and its associated rotational doppler shift, New J. Phys. **10**, 013018 (2008).

[15] C. E. M. Demore, Z. Yang, A. Volovick, S. Cochran, M. P. MacDonald, and G. C. Spalding, Mechanical Evidence of the Orbital Angular Momentum to Energy Ratio of Vortex Beams, Phys. Rev. Lett. **108**, 194301 (2012).

[16] A. Anhäuser, R. Wunenburger, and E. Brasselet, Acoustic Rotational Manipulation Using Orbital Angular Momentum Transfer, Phys. Rev. Lett. **109**, 034301 (2012).

[17] D. Foresti and D. Poulikakos, Acoustophoretic Contactless Elevation, Orbital Transport and Spinning of Matter in Air, Phys. Rev. Lett. **112**, 024301 (2014).

[18] Z. Y. Hong, J. Zhang, and B. W. Drinkwater, Observation of Orbital Angular Momentum Transfer from Bessel-Shaped Acoustic Vortices to Diphasic Liquid-Microparticle Mixtures, Phys. Rev. Lett. **114**, 214301 (2015).

[19] A. Marzo, S. A. Seah, B. W. Drinkwater, D. R. Sahoo, B. Long, and S. Subramanian, Holographic acoustic elements for manipulation of levitated objects, Nat. Commun. **6**, 8661 (2015).

[20] K. Melde, A. G. Mark, T. Qiu, and P. Fischer, Holograms for acoustics, Nature (London) **537**, 518 (2016).

[21] T. Wang, M. Ke, W. Li, Q. Yang, C. Qiu, and Z. Liu, Particle manipulation with acoustic vortex beam induced by a brass

plate with spiral shape structure, Appl. Phys. Lett. **109,** 123506 (2016).

[22] D. Baresch, J. L. Thomas, and R. Marchiano, Orbital Angular Momentum Transfer to Stably Trapped Elastic Particles in Acoustical Vortex Beams, Phys. Rev. Lett. **121,** 074301 (2018).

[23] M. Baudoin, J. C. Gerbedoen, A. Riaud, O. B. Matar, N. Smagin, and J. L. Thomas, Folding a focalized acoustical vortex on a flat holographic transducer: Miniaturized selective acoustical tweezers, Sci. Adv. **5,** (2019).

[24] S. Guo, X. Guo, X. Wang, X. Du, P. Wu, A. Bouakaz, and M. Wan, Manipulation of Nanodroplets Via a Nonuniform Focused Acoustic Vortex, Phys. Rev. Applied **13,** 034009 (2020).

[25] R. Zhang, H. Guo, W. Deng, X. Huang, F. Li, J. Lu, and Z. Liu, Acoustic tweezers and motor for living cells, Appl. Phys. Lett. **116,** 123503 (2020).

[26] B. Sanchez-Padilla, L. Jonusauskas, M. Malinauskas, R. Wunenburger, and E. Brasselet, Direct Mechanical Detection and Measurement of Wave-Matter Orbital Angular Momentum Transfer by Nondissipative Vortex Mode Conversion, Phys. Rev. Lett. **123,** 244301 (2019).

[27] X. Jiang, Y. Li, B. Liang, J.-c. Cheng, and L. Zhang, Convert Acoustic Resonances to Orbital Angular Momentum, Phys. Rev. Lett. **117,** 034301 (2016).

[28] N. Jiménez, R. Picó, V. Sánchez-Morcillo, V. Romero-García, L. M. García-Raffi, and K. Staliunas, Formation of high-order acoustic bessel beams by spiral diffraction gratings, Phys. Rev. E **94,** 053004 (2016).

[29] N. Jiménez, V. Romero-Garca, L. M. Garca-Raffi, F. Camarena, and K. Staliunas, Sharp acoustic vortex focusing by fresnel-spiral zone plates, Appl. Phys. Lett. **112,** 204101 (2018).

[30] R. D. Muelas-Hurtado, J. L. Ealo, and K. Volke-Seplveda, Active-spiral fresnel zone plate with tunable focal length

for airborne generation of focused acoustic vortices, Appl. Phys. Lett. **116,** 114101 (2020).

[31] L. V. King, On the theory of the inertia and diffraction corrections for the rayleigh disc, Proc. R. Soc. A **153,** 17 (1935).

[32] J. B. Keller, Acoustic torques and forces on disks, J. Acoust. Soc. Am. **29,** 1085 (1957).

[33] J.-L. Thomas, R. Marchiano, and D. Baresch, Acoustical and optical radiation pressure and the development of single beam acoustical tweezers, J. Quant. Spectrosc. Radiat. Transfer **195,** 55 (2017).

[34] K. Y. Bliokh and F. Nori, Spin and orbital angular momenta of acoustic beams, Phys. Rev. B **99,** 174310 (2019).

[35] C. Z. Shi, M. Dubois, Y. Wang, and X. Zhang, High-speed acoustic communication by multiplexing orbital angular momentum, Proc. Natl. Acad. Sci. U.S.A. **114,** 7250 (2017).

[36] X. Jiang, B. Liang, J. C. Cheng, and C. W. Qiu, Twisted acoustics: Metasurfaceenabled multiplexing and demultiplexing, Adv. Mater. **30,** 1800257 (2018).

[37] X.-D. Fan, Z. Zou, and L. Zhang, Acoustic vortices in inhomogeneous media, Phys. Rev. Research **1,** 032014 (2019).

[38] X. Li, Y. Li, Q. Ma, G. Guo, J. Tu, and D. Zhang, Principle and performance of orbital angular momentum communication of acoustic vortex beams based on single-ring transceiver arrays, J. Appl. Phys. **127,** 124902 (2020).

[39] V. Fedoseyev, Spin-independent transverse shift of the centre of gravity of a reflected and of a refracted light beam, Opt. Commun. **193,** 9 (2001).

[40] R. Dasgupta and P. Gupta, Experimental observation of spin-independent transverse shift of the centre of gravity of a reflected laguerre–gaussian light beam, Opt. Commun. **257,** 91 (2006).